Single-molecule analysis of phospholipid scrambling by TMEM16F

Rikiya Watanabe[a,1,2], Takaharu Sakuragi[b,1], Hiroyuki Noji[a,2], and Shigekazu Nagata[b,2]

[a]Department of Applied Chemistry, The University of Tokyo, Tokyo 113-8656, Japan; and [b]Laboratory of Biochemistry & Immunology, World Premier International Immunology Frontier Research Center, Osaka University, Osaka 565-0871, Japan

Edited by David A. Weitz, Harvard University, Cambridge, MA, and approved February 11, 2018 (received for review October 12, 2017)

Transmembrane protein 16F (TMEM16F) is a Ca^{2+}-dependent phospholipid scramblase that translocates phospholipids bidirectionally between the leaflets of the plasma membrane. Phospholipid scrambling of TMEM16F causes exposure of phosphatidylserine in activated platelets to induce blood clotting and in differentiated osteoblasts to promote bone mineralization. Despite the importance of TMEM16F-mediated phospholipid scrambling in various biological reactions, the fundamental features of the scrambling reaction remain elusive due to technical difficulties in the preparation of a platform for assaying scramblase activity in vitro. Here, we established a method to express and purify mouse TMEM16F as a dimeric molecule by constructing a stable cell line and developed a microarray containing membrane bilayers with asymmetrically distributed phospholipids as a platform for single-molecule scramblase assays. The purified TMEM16F was integrated into the microarray, and monitoring of phospholipid translocation showed that a single TMEM16F molecule transported phospholipids nonspecifically between the membrane bilayers in a Ca^{2+}-dependent manner. Thermodynamic analysis of the reaction indicated that TMEM16F transported 4.5×10^4 lipids per second at 25 °C, with an activation free energy of 47 kJ/mol. These biophysical features were similar to those observed with channels, which transport substrates by facilitating diffusion, and supported the stepping-stone model for the TMEM16F phospholipid scramblase.

phospholipid scrambling | membrane protein | TMEM16F | single-molecule analysis | microsystem

In eukaryotic cells, the plasma membrane consists of inner and outer leaflets between which phospholipids are asymmetrically distributed. For example, phosphatidylserine (PtdSer) and phosphatidylethanolamine (PtdEtn) are strictly confined to the inner leaflets. This asymmetrical distribution is maintained by flippases (1, 2), and we recently identified the P4-type ATPases ATP11A and ATP11C as the flippases that translocate PtdSer and PtdEtn from the outer leaflet to the inner leaflet in the plasma membrane (3).

Apoptotic cells or activated platelets expose PtdSer through the activities of scramblases, which are activated either by caspase or Ca^{2+} (4). Transmembrane protein 16F (TMEM16F), a member of the TMEM16 family, is a Ca^{2+}-dependent phospholipid scramblase (5) that mediates PtdSer exposure in activated platelets during blood clotting and regulates hydroxyapatite release from osteoblasts during bone mineralization (6, 7). Similar to TMEM16A, which functions as a Ca^{2+}-dependent Cl^- channel (8), Ca^{2+} binds directly to TMEM16F and presumably induces conformational changes (9), resulting in activation of the scrambling reaction. A recent theoretical analysis (10) based on the tertiary structure of the fungal ortholog of TMEM16 (11), along with mutational analysis of mouse TMEM16F (mTMEM16F) (12), suggests a "stepping-stone" model for TMEM16F-mediated phospholipid scrambling, as described in more detail later.

The biophysical features of TMEM16F-mediated lipid scrambling have not been well characterized because the purification of intact TMEM16F is difficult. Moreover, membrane bilayers with asymmetrically distributed phospholipids are challenging to construct, with a few exceptions (13–15). We recently developed microarrays containing membrane bilayers to study membrane transporters at the single-molecule level (16–18). Therefore, in this study, we further developed a microarray system containing asymmetrical membrane bilayers with fluorescently labeled phospholipids in only one leaflet. Additionally, we established a cell line that stably overexpressed mTMEM16F and succeeded in purifying this protein to near homogeneity. By introducing the purified mTMEM16F into the microsystem, we analyzed the functional dynamics of mTMEM16F-mediated phospholipid scrambling at the single-molecule level and found that the scrambling system was remarkably efficient.

Results

Purification of mTMEM16F. mTMEM16F consists of 10 transmembrane segments with cytoplasmic N- and C-terminal tails and a Ca^{2+}-binding site located between transmembrane segments 6, 7, and 8 (9, 11) (Fig. 1*A*). In contrast to transient large-scale production of mTMEM16A (19), the transient overexpression of mTMEM16F in 293T cells caused protein aggregation. To circumvent this, we established a Ba/F3 stable transformant that showed high expression of mTMEM16F in the plasma membrane; that is, Ba/F3 cells were transfected with the expression plasmid carrying Flag-tagged *mTMEM16F* cDNA under the elongation factor-1α promoter and puromycin resistance gene, and stable transformants were selected in the presence of 2 μg/mL puromycin. A monoclonal antibody (mAb) against the fifth extracellular region of mTMEM16F (amino acids 745–825; Fig. 1*A*) recognized cells expressing mTMEM16F. Approximately 1.7% of the population of the transformants expressing high levels of mTMEM16F was sorted by flow cytometry and expanded in the

Significance

Membrane proteins that translocate various compounds across biological membranes play important roles in maintaining intracellular homeostasis in cells. Scramblases are membrane proteins that translocate phospholipids between the inner and outer leaflets of the plasma membrane. However, the mechanisms through which these scramblases translocate phospholipids carrying a hydrophilic residue across the hydrophobic membranes are still unclear. Here, we developed a microsystem containing lipid-bilayer membrane arrays with asymmetrically distributed fluorescent phospholipids. Using this system, we measured phospholipid transport mediated by the TMEM16F scramblase at the single-molecule level, thereby enabling characterization of the biophysical features of phospholipid transport.

Author contributions: R.W., T.S., and S.N. designed research; R.W. and T.S. performed research; R.W., T.S., and S.N. analyzed data; and R.W., H.N., and S.N. wrote the paper.

The authors declare no conflict of interest.

This article is a PNAS Direct Submission.

[1]R.W. and T.S. contributed equally to this work.

[2]To whom correspondence may be addressed. Email: wrikiya@nojilab.t.u-tokyo.ac.jp, hnoji@appchem.t.u-tokyo.ac.jp, or snagata@ifrec.osaka-u.ac.jp.

This article contains supporting information online at www.pnas.org/lookup/suppl/doi:10.1073/pnas.1717956115/-/DCSupplemental.

Published online March 5, 2018.

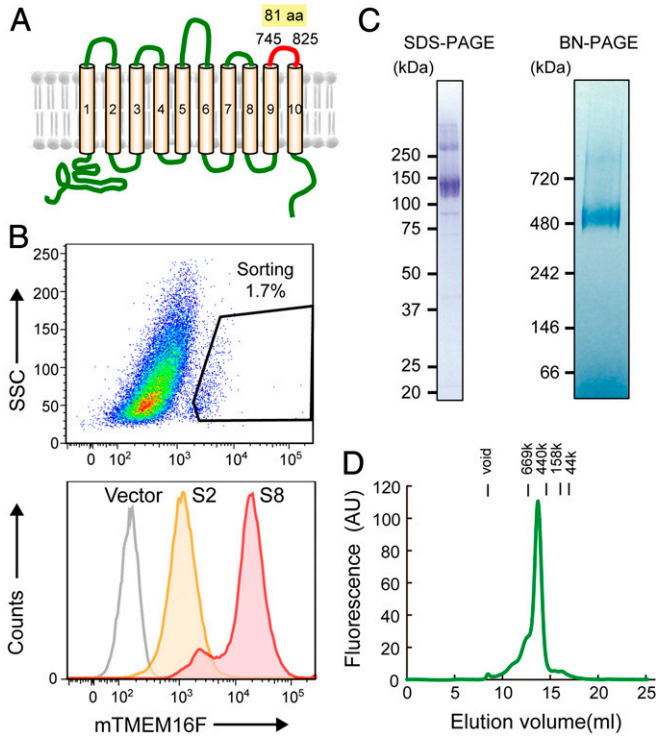

Fig. 1. Transformants overexpressing TMEM16F and purified TMEM16F. (*A*) Schematic structure of the mTMEM16F structure. The fifth extracellular region used as an antigen to prepare mAbs against mTMEM16F is indicated in red. The numbers indicate the positions of the first and last amino acids of the fifth extracellular region. (*B*) Establishment of a Ba/F3 transformant overexpressing mTMEM16F by fluorescence-activated cell sorting (FACS). (*Top*) Original Ba/F3 transformants expressing mTMEM16F were stained with anti-mTMEM16F mAbs, and cells in the boxed area were collected using a FACSAria II. (*Bottom*) Cells sorted twice (S2) or eight times (S8) were stained with anti-mTMEM16F mAbs, and their staining profiles are shown, together with those of the Ba/F3 cells transformed by the empty vector. (*C* and *D*) Biochemical characterization of the purified mTMEM16F. The purified mTMEM16F was analyzed by SDS/PAGE and BN/PAGE (*C*) and gel filtration (*D*) using 1.5 μg, 2.9 μg, and 0.5 μg of protein, respectively. Proteins in SDS/PAGE and BN/PAGE were stained with Coomassie Brilliant Blue, whereas proteins in gel filtration were detected by intrinsic tryptophan fluorescence. Precision Plus Protein Standards (Bio-Rad) and NativeMark Unstained Protein Standards (Thermo Fisher Scientific) were used as molecular weight standards for SDS/PAGE and BN/PAGE, respectively, and their molecular weights are shown on the left. In gel filtration, thyroglobulin (669 kDa), ferritin (440 kDa), aldolase (158 kDa), and ovalbumin (44 kDa) were analyzed. AU, arbitrary unit.

presence of 4 μg/mL puromycin. This procedure (i.e., sorting by flow cytometry and expansion in the presence of increasing concentrations of puromycin) was repeated, resulting in a gradual increase in the expression level of mTMEM16F (Fig. 1*B*). After the ninth sorting, cells that expressed mTMEM16F at a level more than 15-fold that of the original cells were subjected to limiting dilution to obtain a clone (S9-12) showing strong expression of mTMEM16F.

Flag-tagged mTMEM16F was purified from the solubilized membrane fraction of S9-12 transformants by affinity chromatography with anti-Flag mAbs. Briefly, S9-12 cells were subjected to large-scale culture, and the membrane fraction was prepared by ultracentrifugation. After solubilizing the membrane fraction with 1% lauryl maltose neopentyl glycol (LMNG), Flag-tagged mTMEM16F was bound to the anti-Flag mAb and eluted with a linear gradient of LiCl, which strongly improved the purification efficiency compared with conventional stepwise elution with a Flag peptide. Because LMNG bound to proteins is not easily released from the protein (20), the purified mTMEM16F was subjected to the gradient-based detergent removal (GraDeR) procedure (21) to remove the excess LMNG, which was expected to enhance the integration of mTMEM16F into lipid bilayers. Overall, about 150 μg of protein was obtained from a 5-L culture of S9-12.

The final preparation of mTMEM16F was nearly homogeneous in SDS and Blue-native/polyacrylamide gel electrophoresis (BN/PAGE; Fig. 1*C*). The apparent M_r of TMEM16F in SDS/PAGE was 140 kDa, whereas that in BN/PAGE was 520 kDa. The mTMEM16F harbored six *N*-glycosylation sites, which may explain the apparent differences between the M_r in SDS/PAGE and the calculated M_r (108,413.1 Da). Because the apparent size of membrane proteins in BN/PAGE was 1.8-fold larger than the actual size (22), mTMEM16F in the native form was a dimer, consistent with previous results obtained by chemical cross-linking (23). The minor band observed at around 280 kDa in SDS/PAGE was likely to be a dimer that persisted under the mild conditions used for SDS/PAGE (i.e., no heating of the sample in SDS sample buffer). Gel filtration analysis of the purified TMEM16F protein (Fig. 1*D*) indicated that the protein was of high monodispersity, with an apparent M_r of ∼500 kDa. Although the subunit structure of membrane proteins cannot be determined by gel filtration (24), the similar size obtained by BN/PAGE supported that the TMEM16F protein existed as a homodimer.

Formation of Lipid Membranes on Microarrays. Microarrays with more than 10,000 microchambers (diameter: 2.4–8.2 μm, height: 0.5 μm) were fabricated by soft lithography (16) on a hydrophilic glass substrate coated with carbon-fluorine polymer (CYTOP; Asahi-Glass) (Fig. 2*A*). The experimental system consisted of glass substrates with microarrays, a spacer sheet, and a glass block with an access port for sample injection (Fig. S1). To construct phospholipid membranes, the microchambers were first filled with an aqueous solution containing Alexa Fluor 405, which was used to monitor the integrity of lipid bilayers during experiments (Fig. S2*A*). A chloroform solution containing 0.3 mg/mL 1-palmitoyl-2-oleoyl-sn-glycero-3-phosphocholine (POPC) with the indicated amount of acyl-chain–modified fluorescent phospholipids [i.e., 1.0 μg/mL TopFluor-TMR-PS (serine), TopFluor-TMR-PC (choline), and TopFluor-TMR-PE (ethanolamine)] was then infused via the access port. At these concentrations, water-in-oil droplets formed and deposited a lipid monolayer over orifices of microchambers (Fig. S2*B*). Chloroform is the most suitable organic solvent for the formation of a thin lipid membrane on microarrays in a high-throughput manner (15–17). Finally, a second aqueous solution was infused to form another lipid monolayer at the interface with the chloroform solution, which was then deposited over the entire surface of the device (Fig. S2*B*). Thus, bilayers were formed over microchambers containing Alexa Fluor 405, whereas monolayers were formed elsewhere (Fig. 2*A*). Three-dimensional measurements indicated that the fluorescent intensity in microchambers was obviously higher than that on the surface of the polymer (Fig. 2*C*), confirming the membrane geometry in the microarray and suggesting that the outer membrane layers over microchambers, but not the inner layers, were contiguous with the monolayer in other parts of the device (Fig. 2*A*).

To confirm the lamellarity of the membrane, passive transport assays were conducted using α-hemolysin, a toxic membrane protein that specifically binds to unilamellar lipid-bilayer membranes (thickness of ∼4 nm) and forms transmembrane nanopores (diameter: 1–2 nm) (25). For this assay, microchambers encapsulating Alexa Fluor 488 (16, 26) were treated with α-hemolysin (Fig. S3*A*). The rapid decay of the fluorescent intensity indicated (Fig. S3*B*) that Alexa Fluor 488 was diffused through α-hemolysin pores, confirming that the lipid membranes on the microchambers were unilamellar bilayers.

Formation of Asymmetrical Phospholipid Distributions. The fluorescence of phospholipids labeled with TopFluor-TMR in bilayer membranes over microchambers was photobleached to establish

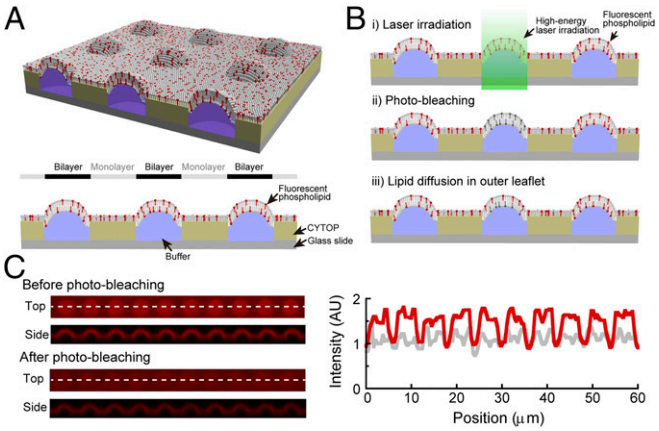

Fig. 2. Microarray assay system for phospholipid scramblase. (*A*) Microchambers fabricated with CYTOP on a glass substrate. Each microchamber was filled with an aqueous solution (purple) and covered with phospholipid bilayers of POPC (gray) and fluorescent phospholipids (red). All other areas were covered by a monolayer of the same phospholipids, the fatty acids of which faced the hydrophobic CYTOP polymer. This monolayer was contiguous with the upper leaflets of bilayers deposited at the top of microchambers. (*B*) Procedures. (*i*) Membrane bilayers formed over microchambers were exposed for a few seconds to a laser to (*ii*) photobleach fluorescently labeled phospholipids (red). (*iii*) Fluorescent lipids diffused into the bilayer from the surrounding area, but were then restricted to the outer layer. (*C*) Confocal fluorescence images of microarrays. (*Left*) Maximum intensity projection (top) and cross-sectional (side) views of TopFluor-TMR-PS (red) before and after photobleaching are shown. (*Right*) Intensity profile of the fluorescence along the dashed lines in the top view before (red) and after (gray) photobleaching is shown. AU, arbitrary unit.

the asymmetrical distribution of the phospholipids by exposure to a high-energy laser at $\lambda = 561$ nm for a few seconds. As shown in Fig. 2 *B* and *C*, the fluorescence in microchambers gradually recovered within several hundred seconds to the same level as on the surrounding surfaces, confirming that the membrane over the microchambers was contiguous with the monolayer in other parts of the device (Fig. 2*A*). This lateral diffusion of phospholipids was temperature-dependent (Fig. S4), with a diffusion coefficient of ~1.0 $\mu m^2 \cdot s^{-1}$ at 25 °C; this value was comparable to that for lateral phospholipid diffusion in planar membranes (27). Notably, the fluorescence recovered over microchambers did not exceed that on surrounding surfaces (Fig. 2*C*), indicating that vertical translocation of phospholipids between the two layers of the membrane did not occur during measurement or was very slow, as also observed in plasma membranes (28). In addition, this result suggested that photobleaching generated an asymmetrical membrane bilayer in which unbleached fluorescent phospholipids were present only in the upper layer. Hence, we concluded that this experimental system was suitable to investigate scramblase activity at the single-molecule level, and that the fluorescent intensity in the microchamber would increase upon phospholipid scrambling.

Phospholipid Scrambling Using mTMEM16F. Because membrane proteins can be integrated as functional proteins into membrane bilayers on microarrays under detergent-free conditions (29), the purified mTMEM16F was diluted in Ca^{2+}- and detergent-free buffer and was injected into a microarray that had been laser-photobleached (Fig. 3*A*). The microsystem was then left to stand for 30 min at room temperature to integrate the protein into membrane bilayers.

We postulated that in the artificially reconstituted system, TMEM16F would be integrated into membrane bilayers with random topology in one functional enzyme per microchamber at low-protein concentrations. To confirm this, Alexa Fluor 555-labeled anti-FLAG antibodies were infused into the microsystem to visualize C-terminally Flag-tagged TMEM16F in membrane bilayers (Fig. S5). In this setup, only TMEM16F molecules outwardly orienting the Flag-tag, for which the Ca^{2+} binding site also showed the same topology, were fluorescently labeled. Observation by total internal reflection fluorescence microscopy (TIRFM) indicated that the fluorescence signals of Alexa Fluor 555 exhibited single-step photobleaching (Fig. S5*B*), confirming that individual Alexa Fluor 555 signals corresponded to single TMEM16F molecules. Next, we counted the number of integrated molecules and found that microchambers loaded with 3.4 μg/mL TMEM16F contained an average of 6×10^{-3} molecules (i.e., a single molecule of TMEM16F was integrated into the membrane bilayer of 0.60% of microchambers; Fig. S5*C*).

For the scrambling assay, 100 μM Ca^{2+} was infused into the microarrays to activate the phospholipid scrambling of TMEM16F. In this setup, only TMEM16F molecules outwardly orienting the Ca^{2+} binding site were activated by Ca^{2+} infusion. The fluorescent intensity of the bilayer membrane gradually increased upon Ca^{2+} infusion (Fig. 3 *B* and *C*) in 0.58% of microchambers loaded with 3.4 μg/mL TMEM16F (Fig. 3*D*), which coincided with the fraction of microchambers containing a single molecule of TMEM16F (Fig. S5*C*). The percentage of microchambers showing a positive response increased in proportion to the concentration of TMEM16F loaded between 0.7 and 6.3 μg/mL (Fig. 3*D* and Fig. S6) and in proportion to the size of the microchamber (and hence the membrane area; Fig. 3*E* and Fig. S7). These properties are typical of a single-molecule digital assay (16, 30, 31) and suggested that a single functional unit mediated the increase in fluorescence in each microchamber.

The fluorescent intensity at microchambers loaded with TMEM16F gradually increased to reach the original intensity level before photobleaching (Fig. 3*C*), irrespective of the phospholipid composition of the membranes (Figs. S8 and S9). This suggested that the fluorescent phospholipids were translocated from the outer layer to the inner layer, which was followed by lateral diffusion from the surrounding monolayer. This increase in fluorescence was not observed in microchambers not loaded with TMEM16F or in those loaded with the purified TMEM16A, a Ca^{2+}-dependent Cl^- channel (19) (Fig. S10).

TMEM16F-mediated phospholipid scrambling is known to be Ca^{2+}-dependent, nonspecific for phospholipids, and inhibited by tannic acid or epigallocatechin gallate (EGCg) (23). Accordingly, only a very small percentage (0.09%) of TMEM16F-loaded microchambers gained fluorescence in the absence of Ca^{2+}, and this percentage increased to 0.6% after supplementation with 100 μM Ca^{2+} (Fig. 3*F*). In addition, increased fluorescence was observed at similar efficiencies for various fluorescence substrates (i.e., TopFluor-TMR-PS, TopFluor-TMR-PC, TopFluor-TMR-PE) (Fig. 3*G*), and this increase was fully blocked with 1.0 μM tannic acid or EGCg (Fig. 3*F*). Collectively, these results strongly indicated that TMEM16F supported the translocation of fluorescent phospholipids between membrane bilayers at the single-molecule level. Notably, when loaded microchambers that had already gained more fluorescence than the surrounding area were laser-photobleached a second time, these microchambers gradually regained fluorescence up to the original level in the presence of 100 μM Ca^{2+}, but not in the presence of 100 μM Ca^{2+} plus 1.0 μM EGCg or tannic acid (Fig. 3*C* and Fig. S11), indicating that phospholipid scrambling by TMEM16F could be triggered more than one time in our microarrays.

Kinetic Analysis of TMEM16F-Mediated Phospholipid Scrambling. Although the percentage of microchambers with scramblase activity increased as the area of the bilayer membrane increased (Fig. 3*E*), the scrambling process also slowed down (Fig. 4*A*). Because TMEM16F-mediated scrambling is reversible (5), the reaction should follow

$$[Lipid_{out}] \underset{k}{\overset{k}{\rightleftarrows}} [Lipid_{in}],$$

where k is the rate constant and $[Lipid_{out}]$ and $[Lipid_{in}]$ are the concentrations of fluorescent lipids at the outer and inner layers,

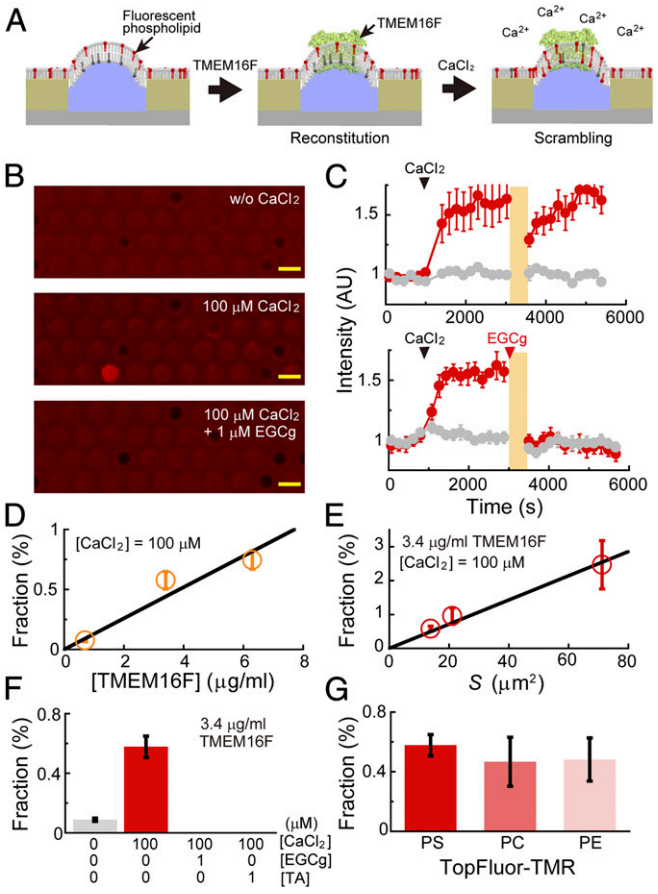

Fig. 3. Phospholipid scrambling by a single TMEM16F molecule. (*A*) TMEM16F was incorporated into the asymmetrical membrane bilayers with fluorescent phospholipids (red). Addition of $CaCl_2$ initiated phospholipid scrambling, followed by lateral diffusion of unbleached phospholipids from surrounding areas, increasing the fluorescence intensity in microchambers. (*B*) Purified TMEM16F was loaded at 3.4 μg/mL, and scrambling was initiated with 100 μM $CaCl_2$. Subsequently, the asymmetrical membrane bilayers were again formed by laser irradiation, and the scambling was assayed by injecting 100 μM $CaCl_2$ in the presence of 1 μM EGCg. Maximum intensity projections of confocal images of TopFluor-TMR-PS (red) obtained from the same microchambers before (*Top*) and after addition of 100 μM $CaCl_2$ (*Middle*) or 100 μM $CaCl_2$ + 1 μM EGCg (*Bottom*) are shown. (Scale bars: 5 μm.) AU, arbitrary unit. (*C*) Time course of TMEM16F-mediated phospholipid scrambling. Lipid bilayers with (red) or without (gray) TMEM16F were treated with 100 μM $CaCl_2$ (black arrowheads), and fluorescence from TopFluor-TMR-PS was followed over time. Subsequently, the microchambers were reexposed for a few seconds to a laser at time points marked in orange, with (*Bottom*) or without (*Top*) prior injection of 1 μM EGCg (red arrowhead). (*D*) Microarrays with fluorescent TopFluor-TMR-PS in the outer layer were loaded with 0.7, 3.4, or 6.3 μg/mL TMEM16F in buffer containing 100 μM $CaCl_2$. The percentage of chambers with scramblase activity was plotted as orange circles, with SDs as error bars. The black line is a linear regression. (*E*) Percentage of chambers with scramblase activity against the membrane area (*S*). Microarrays with TopFluor-TMR-PS were loaded with 3.4 μg/mL TMEM16F in buffer containing 100 μM $CaCl_2$. The black line is the linear regression. (*F*) Percentage of microchambers with scramblase activity against the concentration of Ca^{2+} or inhibitors. Microarrays with TopFluor-TMR-PS were loaded with 3.4 μg/mL TMEM16F in a buffer containing the indicated concentrations of $CaCl_2$ and inhibitors [EGCg and tannic acid (TA)]. (*G*) Percentage of chambers with scramblase activity against fluorescence substrates: TopFluor-TMR-PS (red), TopFluor-TMR-PC (light red), or TopFluor-TMR-PE (pink). Microarrays were loaded with 3.4 μg/mL TMEM16F in buffer containing 100 μM $CaCl_2$.

respectively. Notably, $[Lipid_{out}]$ is considered constant because it is contiguous with a large lipid monolayer in surrounding areas. Since the fluorescent intensity over the microchamber (*FI*) is proportional to the concentration of fluorescent lipids, *FI* is thus determined as a function of time *t*;

$$FI = FI_{out} + FI_{in} \cdot [1 - \exp(-k^* \cdot t)], \quad [1]$$

$$k^* = \frac{k}{\eta} \cdot \frac{1}{S}, \quad [2]$$

where FI_{out} and FI_{in} are the fluorescent intensities of the outer and inner layers, respectively; *S* is the area of the membrane over the microchambers; and η is the number of lipid molecules per unit area of the monolayer ($\sim 2.0 \times 10^6$ per square micron), as determined previously (32). Fitting the time course in Fig. 4*A* to Eq. **1** demonstrated k^*, the rate constant of fluorescent increase at 25 °C. As expected from Eq. **2**, k^* was inversely proportional to *S* (Fig. 4*B*), demonstrating that *k*, the rate of TMEM16F-mediated lipid transport, was 4.5×10^4 lipids per second at 25 °C (Fig. 4*C*); this value was $\sim 10^8$-fold faster than spontaneous vertical lipid flip-flop across membrane bilayers (28). Importantly, the *k* value did not differ between fluorescence substrates (i.e., TopFluor-TMR-PS, TopFluor-TMR-PC, and TopFluor-TMR-PE; Fig. 4*C*), indicating that TMEM16F did not distinguish between head group moieties of phospholipids and confirming that TMEM16F nonspecifically scrambled phospholipids. In addition, the *k* value did not differ at different lipid compositions [e.g., in the absence or presence of phosphatidylinositol (PI); Fig. 4*C*], suggesting that the lipid composition did not significantly affect the scrambling activity of TMEM16F.

TMEM16F-mediated scrambling was temperature-dependent (Fig. 5*A* and Fig. S12), with *k* values of 1.4×10^4 and 7.1×10^4 lipids per second at 16 °C and 35 °C, respectively. The corresponding Arrhenius plot fit well to a linear function (Fig. 5*B*), indicating that TMEM16F-mediated lipid transport was governed by a single rate-limiting step, at least from 16 to 31 °C. The thermodynamic parameters of this rate-limiting step were as follows: $\Delta G^{\ddagger} = 47$ kJ/mol, $\Delta H^{\ddagger} = 82$ kJ/mol, and $T\Delta S^{\ddagger} = 35$ kJ/mol at 25 °C (Fig. 5*B*, *Inset*). The $\Delta G^{\ddagger}$ value for spontaneous vertical lipid flip-flop was ~100 kJ/mol (28), suggesting that TMEM16F significantly reduces the activation free energy.

Discussion

In this study, we demonstrated the single-molecule analysis of phospholipid scrambling of TMEM16F. The rate of phospholipid transport by a single molecule of TMEM16F was estimated as $k = 4.5 \times 10^4$ lipids per second at 25 °C (i.e., 2.2×10^{-5} s was required to translocate a single phospholipid across the membrane bilayer). Compared with other membrane transporters, the rate of phospholipid transport by TMEM16F was faster than those of carrier proteins, such as F-type (16) and P-type (33) ATPases ($<10^2$ molecules per second), and similar to those of channel proteins, such as KirBac1.1 (34) ($>10^5$ molecules per second). Carrier proteins transport substrates by coupling with conformational changes fueled by enzymatic reactions, for example, ATP hydrolysis, which is presumably a rate-limiting step of transport activity (35, 36). In contrast, channel proteins form a transmembrane pore (conducting pathway), allowing substrates to diffuse very rapidly (34, 37). Thus, the rate of phospholipid transport by TMEM16F was reasonable because TMEM16F-mediated scrambling did not require any energy input (i.e., a diffusion-limiting process). These findings supported the idea that, similar to ligand-gated channels (38), TMEM16F provided a cleft (conducting pathway) for phospholipid diffusion upon Ca^{2+} binding (10, 12).

To estimate the diffusion properties, we constructed a simple physical model of phospholipid scrambling of TMEM16F: 1D diffusion of phospholipids across the cleft of TMEM16F. The time required for phospholipids to travel across the membranes was written as $t = \lambda^2/D$, where λ and *D* are the thickness of the membrane bilayer (~4 nm) and the diffusion coefficient of the phospholipid,

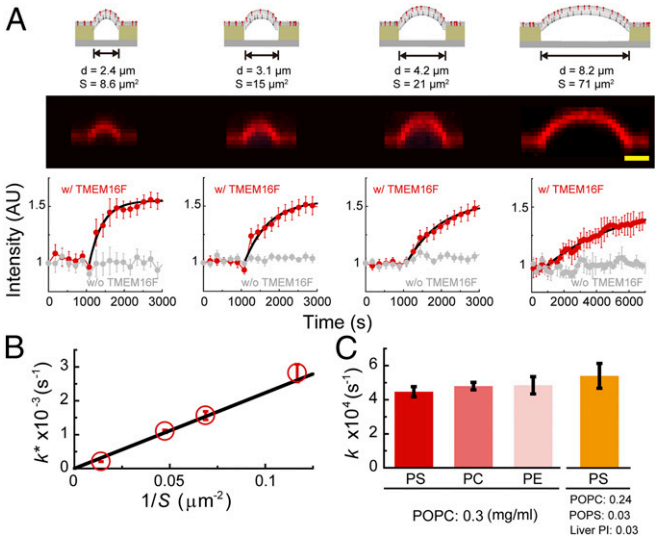

Fig. 4. Biophysical characterization of TMEM16F-mediated scrambling. (*A*) Area (*S*) of the bilayer membrane was calculated (*Top*) from 3D confocal fluorescence images (*Middle*). (Scale bar: 2.5 μm.) (*Bottom*) Microarrays with membrane bilayers of the indicated areas were loaded with (red) or without (gray) 3.4 μg/mL TMEM16F in a buffer containing 100 μM $CaCl_2$, and TopFluor-TMR-PS was followed for the indicated times. Experiments were repeated 24–166 times, and average values from 389 to 20,280 microchambers are plotted with SDs. Black curves are fits to the single-exponential function $y = C_1 + C_2 \times (1 - \exp[-k \times (t - 1{,}000)])$. AU, arbitrary unit; d, diameter of chamber. (*B*) Rate constant of fluorescence increase (*k**) of TopFluor-TMR-PS was plotted against the inverse of membrane area (1/*S*). Data are from at least 380 microchambers in 16 independent experiments, and average values are shown as red circles with SDs. The black line is a linear regression. (*C*) Values of *k* determined at various lipid compositions: 0.3 mg/mL POPC with 0.001 mg/mL TopFluor-TMR-PS (red), TopFluor-TMR-PC (light red), or TopFluor-TMR-PE (pink); 0.24 mg/mL POPC; 0.03 mg/mL POPS; and 0.03 mg/mL liver PI with 0.001 mg/mL TopFluor-TMR-PS (orange).

respectively. From this equation, we obtained a *D* value as 0.7 $\mu m^2 \cdot s^{-1}$ in the cleft of TMEM16F; this value was similar to that of lateral diffusion in membrane bilayers (i.e., 1.0 $\mu m^2 \cdot s^{-1}$) (27) (Fig. S4). Thus, TMEM16F may scramble phospholipids in a manner similar to lateral diffusion in membrane bilayers.

Recent computational and biochemical studies have proposed a stepping-stone model for TMEM16F-mediated phospholipid scrambling (10, 12). In this model, phospholipids bind to positively charged residues located on the transmembrane segment of TMEM16F (stepping stones) via electrostatic interactions with the phosphate moiety of the head group and move stepwise through the membrane bilayers. We found that the head group moieties of phospholipids (i.e., PS, PC, PE) did not affect the scramblase activity of TMEM16F, supporting that only the phosphate moiety forming an electrostatic interaction played an important role for scrambling of phospholipids in the stepping-stone model. The formation of electrostatic interactions induced a negative entropy change, and its disruption induced a positive entropy change. The increase in entropy ($T\Delta S^{\ddagger}$) by 35 kJ/mol in the scrambling reaction (Fig. 5*B*) implied that phospholipid transport may be rate-limited by the release of lipid molecules from stepping stones in TMEM16F.

In this study, we fabricated a microarray with more than 10,000 microchambers lidded by asymmetrical membrane bilayers and measured phospholipid scrambling by a single TMEM16F molecule. The microarray will enable more detailed investigation of this process and will expand the versatility of scramblase assays to other TMEM16 proteins (7), some of which are localized to the endoplasmic reticulum and could not be analyzed by cell-based assays. In addition, the device developed in this study will be useful to measure the phospholipid-translocation activity of other membrane proteins, such as caspase-dependent scramblases, floppases, and flippases, at the single-molecule level (39, 40). Finally, mammalian membrane proteins are often difficult to produce at a large scale. Here, by repeating fluorescence-activated cell sorting (FACS) with mAbs that recognized the extracellular region of TMEM16F, we established a cell line overexpressing TMEM16F and developed a convenient purification procedure. This procedure could have applications in the purification of other membrane proteins.

Materials and Methods

Materials. Alexa Fluor dyes 405, 488, and 555 were purchased from Thermo Fisher Scientific. POPC and 1-palmitoyl-2-oleoyl-*sn*-glycero-3-phospho-L-serine (POPS) were purchased from NOF Co., and bovine liver PI, TopFluor-TMR-PS, TopFluor-TMR-PC, and TopFluor-TMR-PE were from Avanti Polar Lipid. EGCg and tannic acid were purchased from Nacalai Tesque and Wako Chemicals, respectively.

Fabrication of Microchamber Arrays. CYTOP (Asahi-Glass) was coated on a glass cover slide (32 mm × 24 mm; Matsunami) by using the spin-coater (MS-B100, Mikasa) at 4,000 rpm for 30 s and baked for 1 h at 180 °C. The thickness of the CYTOP layer was 0.5 μm. Photolithography was then performed using a positive photoresist (AZP4903; AZ Electronic Materials) to pattern-mask structures on the CYTOP layer. Subsequently, the resist-patterned substrate was dry-etched with O_2 plasma using a reactive ion etching system (RIE-10NR; Samco) to expose an array of hydrophilic SiO_2 glass. Finally, the substrate was cleaned and rinsed with acetone and isopropyl alcohol to remove the photoresist layer. The fabrication success rate was 100%. Fig. 2 and Fig. S1 illustrate the design of the fabricated microchamber array.

Formation of Lipid Membrane. The flow cell (~10 μL) was constructed by assembling a glass slide with microchambers, a spacer sheet (Frame-Seal; BIO-RAD), and a glass block with a sample injection port (length/width/height = 20 mm/20 mm/5 mm) (Fig. S1). The microchambers were first filled with 10 μL of buffer A [4 mM Tris·HCl buffer (pH 7.5), 30 mM NaCl] containing fluorescent dyes (20 μM Alexa Fluor 405 or 1 μM Alexa Fluor 488). Then, 10 μL of chloroform solution containing phospholipids (0.3 $mg \cdot mL^{-1}$ POPC with 1.0 $mg \cdot mL^{-1}$ TopFluor-TMR-PS, TopFluor-TMR-PC, or TopFluor-TMR-PE; 0.24 $mg \cdot mL^{-1}$ POPC; 0.03 $mg \cdot mL^{-1}$ POPS; and 0.03 $mg \cdot mL^{-1}$ liver PI with 1.0 $mg \cdot mL^{-1}$ TopFluor-TMR-PS) was then infused into the flow cell via the access port. Finally, 190 μL of buffer B [2 mM Tris·HCl buffer (pH 7.5), 15 mM NaCl] was infused to form lipid membranes.

Imaging. Fluorescent time-lapse recordings for passive transport and phospholipid scramblase assays were acquired under a confocal microscope system fitted with photomultiplier tubes and a 60× objective lens (A1R; Nikon). Alexa Fluor 405 and Alexa Fluor 488 were excited at 405 nm and 488 nm, respectively, and phospholipids labeled with TopFluor-TMR were excited at 561 nm. Fluorescent intensities were analyzed in NIS Elements (Nikon). Single-molecule detection of fluorescently labeled TMEM16F was performed

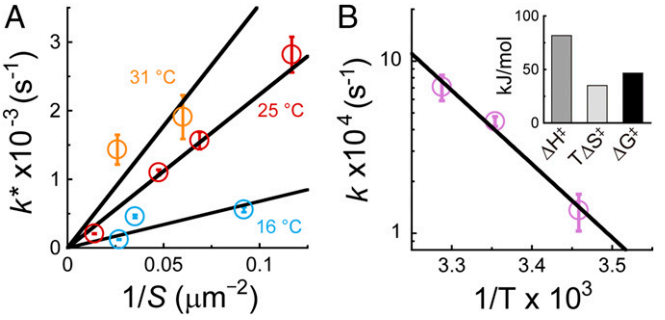

Fig. 5. Temperature dependence of TMEM16F-mediated scrambling. (*A*) Rate constant of fluorescence increase (*k**) represented by orange, red, and blue circles was plotted against the inverse of the membrane area (1/*S*). Data in blue, red, and orange were obtained using TopFluor-TMR-PS at 16 °C, 25 °C, and 31 °C, respectively. Black lines are linear regressions. (*B*) Arrhenius plot for TMEM16F-mediated phospholipid scrambling, with *k* values from *A* (purple). The solid line represents linear regression. (*Inset*) Thermodynamic parameters at 25 °C, as determined from the plot.

under a TIRFM (IX71; Olympus) microscope equipped with an electron-multiplying CCD (iXon; Andor) and a 60× objective lens (N.A. = 1.49; Olympus). The Flag-TMEM16F was labeled with anti-Flag Alexa Fluor 555 and excited at 532 nm. The laser power at the optical inlet of the microscope was 5.7 mW. Fluorescent intensity was analyzed by ImageJ (NIH).

Fluorescence Recovery. To measure fluorescence recovery after photobleaching, the microchambers and flow cell were first filled with buffer A containing 20 μM Alexa Fluor 405, followed by buffer B. The labeled phospholipids were then photobleached for a few seconds at $\lambda = 561$ nm, using a laser-scanning confocal microscope (A1R; Nikon). To assay scramblase activity, bilayer membranes were formed, photobleached as described above, and loaded with TMEM16F for 30 min. Scrambling was initiated by injecting buffer B containing $CaCl_2$, and fluorescence images were recorded at 200-s intervals. Some reactions were performed in the presence of EGCg or tannic acid as indicated.

Passive Transport Assay. The microchambers and flow cell were first filled with buffer A containing 1 μM Alexa Fluor 488 and buffer B, respectively. After the lipid membrane was formed, buffer B containing 0.5 μg/mL α-hemolysin (HT101; Toxin Co.) was injected into the flow cell, and fluorescence images were recorded at 30-s intervals.

Single-Molecule Fluorophore Assay. The microchambers and flow cell were first filled with buffer A and buffer B, respectively. After lipid membrane formation, buffer B containing 3.4 μg/mL TMEM16F was injected into the flow cell. After 30 min, buffer B was injected to flush the residual TMEM16F molecules and buffer C [10 mM Tris·HCl buffer (pH 7.5), 75 mM NaCl] was injected to apply osmotic pressure for depressing the bilayer membranes onto the bottom surface of microchambers, allowing visualization of fluorophores with TIRFM (41). Next, buffer C containing 20 μg/mL anti-Flag Alexa Fluor 555 was injected to conjugate Alexa Fluor 555–TMEM16F complex. After 10 min, buffer C was injected to flash the residual anti-Flag Alexa Fluor 555. Fluorescence images were recorded at 30 frames per second.

ACKNOWLEDGMENTS. We thank Drs. Y. Baba and H. Tsunoda of Chugai Pharmaceutical Co. for providing the anti-mTMEM16F mAb; Drs. J. Suzuki, K. Ishihara, and N. Soga for helpful discussions; and R. Suzuki, S. Suzuki, E. Chiyoda, and Dr. Y. Minagawa for technical support. This work was supported by a Grant-in-Aid for Scientific Research (JP17H03660, JP15H05591) from the Japan Society for the Promotion of Science, a Precursory Research for Embryonic Science and Technology (PRESTO) Grant (JPMJPR13LC) from the Japan Science and Technology Agency, a Precursory Research for Innovative Medical Care (PRIME) Grant (JP17gm0910020) from the Japan Agency for Medical Research and Development, a research grant from Astellas Foundation for Research on Metabolic Disorders, and a research grant from the Foundation of Advanced Technology Institute (to R.W.). Additional support was provided by a Grant-in-Aid for Scientific Research (JP15H05785) from the Japan Society for the Promotion of Science and by Core Research for Evolutional Science and Technology (Grant JPMJCR14M4) from Japan Science Technology (to S.N.).

1. Leventis PA, Grinstein S (2010) The distribution and function of phosphatidylserine in cellular membranes. *Annu Rev Biophys* 39:407–427.
2. Balasubramanian K, Schroit AJ (2003) Aminophospholipid asymmetry: A matter of life and death. *Annu Rev Physiol* 65:701–734.
3. Segawa K, et al. (2014) Caspase-mediated cleavage of phospholipid flippase for apoptotic phosphatidylserine exposure. *Science* 344:1164–1168.
4. Segawa K, Nagata S (2015) An apoptotic 'eat me' signal: Phosphatidylserine exposure. *Trends Cell Biol* 25:639–650.
5. Suzuki J, Umeda M, Sims PJ, Nagata S (2010) Calcium-dependent phospholipid scrambling by TMEM16F. *Nature* 468:834–838.
6. Pedemonte N, Galietta LJV (2014) Structure and function of TMEM16 proteins (anoctamins). *Physiol Rev* 94:419–459.
7. Nagata S, Suzuki J, Segawa K, Fujii T (2016) Exposure of phosphatidylserine on the cell surface. *Cell Death Differ* 23:952–961.
8. Caputo A, et al. (2008) TMEM16A, a membrane protein associated with calcium-dependent chloride channel activity. *Science* 322:590–594.
9. Ishihara K, Suzuki J, Nagata S (2016) Role of Ca(2+) in the stability and function of TMEM16F and 16K. *Biochemistry* 55:3180–3188.
10. Bethel NP, Grabe M (2016) Atomistic insight into lipid translocation by a TMEM16 scramblase. *Proc Natl Acad Sci USA* 113:14049–14054.
11. Brunner JD, Lim NK, Schenck S, Duerst A, Dutzler R (2014) X-ray structure of a calcium-activated TMEM16 lipid scramblase. *Nature* 516:207–212.
12. Gyobu S, Ishihara K, Suzuki J, Segawa K, Nagata S (2017) Characterization of the scrambling domain of the TMEM16 family. *Proc Natl Acad Sci USA* 114:6274–6279.
13. Pautot S, Frisken BJ, Weitz DA (2003) Engineering asymmetric vesicles. *Proc Natl Acad Sci USA* 100:10718–10721.
14. Iwamoto M, Oiki S (2015) Contact bubble bilayers with flush drainage. *Sci Rep* 5:9110.
15. Watanabe R, Soga N, Yamanaka T, Noji H (2014) High-throughput formation of lipid bilayer membrane arrays with an asymmetric lipid composition. *Sci Rep* 4:7076.
16. Watanabe R, et al. (2014) Arrayed lipid bilayer chambers allow single-molecule analysis of membrane transporter activity. *Nat Commun* 5:4519.
17. Soga N, Watanabe R, Noji H (2015) Attolitre-sized lipid bilayer chamber array for rapid detection of single transporters. *Sci Rep* 5:11025.
18. Watanabe R, Soga N, Hara M, Noji H (2016) Arrayed water-in-oil droplet bilayers for membrane transport analysis. *Lab Chip* 16:3043–3048.
19. Dang S, et al. (2017) Cryo-EM structures of the TMEM16A calcium-activated chloride channel. *Nature* 552:426–429.
20. Chung KY, et al. (2012) Role of detergents in conformational exchange of a G protein-coupled receptor. *J Biol Chem* 287:36305–36311.
21. Hauer F, et al. (2015) GraDeR: Membrane protein complex preparation for single-particle cryo-EM. *Structure* 23:1769–1775.
22. Heuberger EH, Veenhoff LM, Duurkens RH, Friesen RH, Poolman B (2002) Oligomeric state of membrane transport proteins analyzed with blue native electrophoresis and analytical ultracentrifugation. *J Mol Biol* 317:591–600.
23. Suzuki T, Suzuki J, Nagata S (2014) Functional swapping between transmembrane proteins TMEM16A and TMEM16F. *J Biol Chem* 289:7438–7447.
24. Korepanova A, Matayoshi ED (2012) HPLC-SEC characterization of membrane protein-detergent complexes. *Curr Protoc Protein Sci* Chapter 29:Unit 29.5.1–12.
25. Song L, et al. (1996) Structure of staphylococcal alpha-hemolysin, a heptameric transmembrane pore. *Science* 274:1859–1866.
26. Tonnesen A, Christensen SM, Tkach V, Stamou D (2014) Geometrical membrane curvature as an allosteric regulator of membrane protein structure and function. *Biophys J* 106:201–209.
27. Kalb E, Frey S, Tamm LK (1992) Formation of supported planar bilayers by fusion of vesicles to supported phospholipid monolayers. *Biochim Biophys Acta* 1103: 307–316.
28. Anglin TC, Conboy JC (2009) Kinetics and thermodynamics of flip-flop in binary phospholipid membranes measured by sum-frequency vibrational spectroscopy. *Biochemistry* 48:10220–10234.
29. Watanabe R, Soga N, Noji H (2015) Novel nano-device to measure voltage-driven membrane transporter activity. *IEEE Trans NanoTechnol* 15:70–73.
30. Zhang Y, Noji H (2017) Digital bioassays: Theory, applications, and perspectives. *Anal Chem* 89:92–101.
31. Kim D, Wei Q, Kong JE, Ozcan A, Di Carlo D (2015) Research highlights: Digital assays on chip. *Lab Chip* 15:17–22.
32. Nagle JF, Tristram-Nagle S (2000) Structure of lipid bilayers. *Biochim Biophys Acta* 1469:159–195.
33. Veshaguri S, et al. (2016) Direct observation of proton pumping by a eukaryotic P-type ATPase. *Science* 351:1469–1473.
34. Wang S, Vafabakhsh R, Borschel WF, Ha T, Nichols CG (2016) Structural dynamics of potassium-channel gating revealed by single-molecule FRET. *Nat Struct Mol Biol* 23: 31–36.
35. Turina P, Samoray D, Gräber P (2003) H+/ATP ratio of proton transport-coupled ATP synthesis and hydrolysis catalysed by CF0F1-liposomes. *EMBO J* 22:418–426.
36. Zhang Z, et al. (2000) Detailed characterization of the cooperative mechanism of $Ca^{(2+)}$ binding and catalytic activation in the $Ca^{(2+)}$ transport (SERCA) ATPase. *Biochemistry* 39:8758–8767.
37. Shimizu H, et al. (2008) Global twisting motion of single molecular KcsA potassium channel upon gating. *Cell* 132:67–78.
38. Plested AJ (2016) Structural mechanisms of activation and desensitization in neurotransmitter-gated ion channels. *Nat Struct Mol Biol* 23:494–502.
39. Hankins HM, Baldridge RD, Xu P, Graham TR (2015) Role of flippases, scramblases and transfer proteins in phosphatidylserine subcellular distribution. *Traffic* 16:35–47.
40. Bevers EM, Williamson PL (2016) Getting to the outer leaflet: Physiology of phosphatidylserine exposure at the plasma membrane. *Physiol Rev* 96:605–645.
41. Tokunaga M, Kitamura K, Saito K, Iwane AH, Yanagida T (1997) Single molecule imaging of fluorophores and enzymatic reactions achieved by objective-type total internal reflection fluorescence microscopy. *Biochem Biophys Res Commun* 235: 47–53.